Stanford Exploration Project, Report 103, April 27, 2000, pages 205–??

Estimation of AVO attributes sensitivity to velocity uncertainty using forward modeling: a progress report

Carmen Mora and Biondo Biondi[1]

ABSTRACT

We investigate the sensitivity of AVO attributes to uncertainty in migration velocity in a synthetic dataset. The synthetic data was built using a earth model with typical rock properties from a real North Sea turbidite field. The model includes a thick overburden layer with complex velocity anomalies. We examine the sensitivity of AVO response due to the presence of this complex layer and quantify the influence of migration velocity errors in the AVO signature. Results show that AVO gradient attribute is more sensitive to velocity errors than AVO intercept attribute. For velocity errors up to 5% we see a maximum of AVO intercept errors of 34%, whereas for velocity errors of only 1%, the inversion of AVO gradient attribute has an error of 185%. Further work is needed to evaluate the influence of observed boundary artifacts on these results.

INTRODUCTION

The variation of seismic reflection coefficients with offset can be used as a direct hydrocarbon indicator (Ostrander, 1984; Swan, 1993), which is supported in the AVO analysis theory. AVO analysis requires previous prestack migration of the data, and velocity estimation is a key factor for this imaging problem. Velocity estimation affects the AVO response because it modifies the position of the events and the resulting amplitude values (Grubb and Tura, 1997). Because of the difficulty of estimating velocity models in complex areas, it is important to understand the sensitivity of AVO attributes to variation in velocity models. Mora and Biondi (1999) explore the relationship between velocity uncertainty and AVO-related seismic attributes using a real dataset. A conclusion from that work is that is important to investigate this problem using a synthetic model that allows more control over the data, which is needed to obtain a quantitative measure of the uncertainties.

In this work we do seismic modeling using typical rock properties from a real North Sea turbidite field. As is mentioned in (Avseth et al., 1999), this field has been problematic because of complex sand distribution and non-reservoir sand anomalies. Two of the three most recent exploration wells failed to encounter reservoir sands in locations where poststack seismic amplitudes indicated reservoir sands. Avseth et al. (1999) suggest that AVO analysis in this field can help to discriminate sands from other lithofacies. However, because of the presence of

[1]**email:** cmora@sep.stanford.edu, biondo@sep.stanford.edu

complex velocity anomalies in the overburden, it is desirable to have a estimation of the uncertainty in the AVO response; in other words, how reliable is the lithology discrimination from AVO analysis given the presence of a complex overburden zone?

In this paper, we do forward modeling, simulating an earth model with an overburden that includes complex velocity anomalies. We generate several migration-velocity realizations by introducing coherent percentage velocity errors in the overburden zone of the original velocity model. We migrate the synthetic data using each velocity realization, and measure the variability in the resulting gradient and intercept AVO attributes that results from the velocity error.

ELASTIC MODELING

To investigate the effect of velocity anomalies in AVO attributes, we generated two synthetic datasets using a finite-difference elastic modeling program. Below is a description of the earth models simulated and the resulting synthetic data.

Models

The two 2-D synthetic datasets were computed assuming an earth model that includes

- A 1.8 km thick overburden.
- A 0.2 km cap rock layer (shale).
- A 0.2 km target zone with three different lithologies for comparison (cemented brine sands, cemented oil sands, and tuff).

Figure 1 shows the P-wave velocity for both models. In model 1, the overburden contains two flat layers with constant elastic properties on each layer, whereas model 2 includes a zone of complex velocity anomalies in the overburden. The rock properties for the model were taken from real well logs of a North Sea field. Typical values for different lithologies at this field are listed in Table 1.

Lithology	V_p (km/s)	V_s (km/s)	ρ (g/cm^3)
Shale	2.4	0.95	2.25
Cemented brine sands	3.1	1.55	2.15
Uncemented brine sands	2.6	1.3	2.1
Cemented oil sands	2.9	1.6	2.05
Uncemented oil sands	2.35	1.33	2
Volcanic ash (tuff)	2.75	1.23	2.2
Limestone	4	2	2.4

Table 1. Typical rock properties for different lithologies at the North Sea.

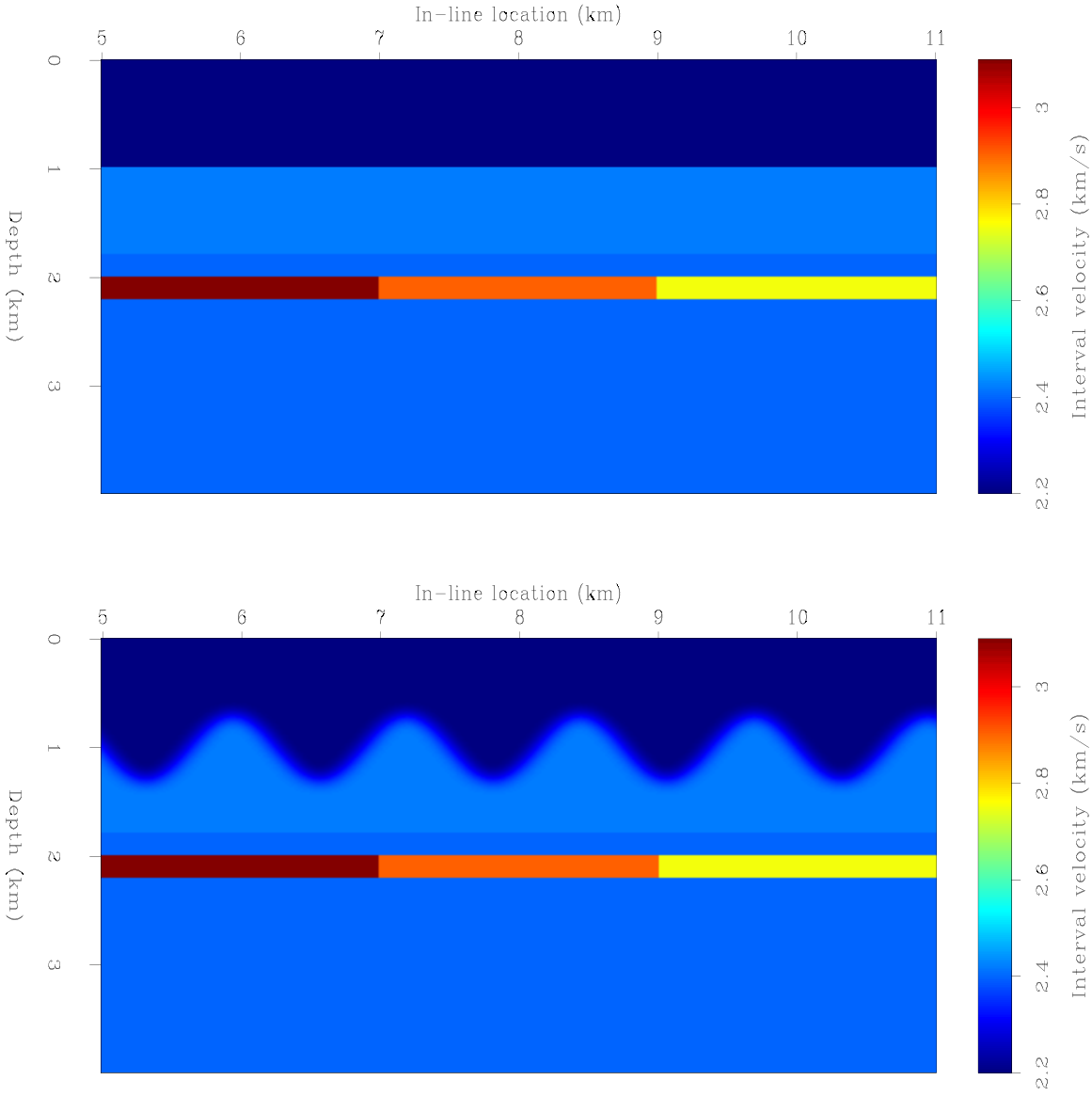

Figure 1: P-wave velocity models used to generate the synthetic data. Model 1 (top): overburden with flat layers, model 2 (bottom): overburden with velocity anomalies. cmora1-model [CR]

Average values for overburden properties in the field are $V_p = 2.2$ km/s, $V_s = 0.75$ km/s, $\rho = 2.15$ (g/cm^3).

In model 1, overburden properties above the flat interface were taken to be the average values indicated above; overburden properties below the interface were the average values with a 10% increase. For model 2, we introduced lateral velocity anomalies by including a smoothed sinusoidal interface between the two layers.

Synthetic seismograms

The synthetic data was generated using an explosive source and a Ricker2 wavelet with a fundamental frequency of 22.5 Hz. The source/receiver offsets ranged from 16 m (minimum offset) to 3.6 km (maximum offset). Figure 2 shows a shot gather at in-line location=5 km for each model; note that the events in model 2 are not perfect hyperboles due to the lateral velocity variations.

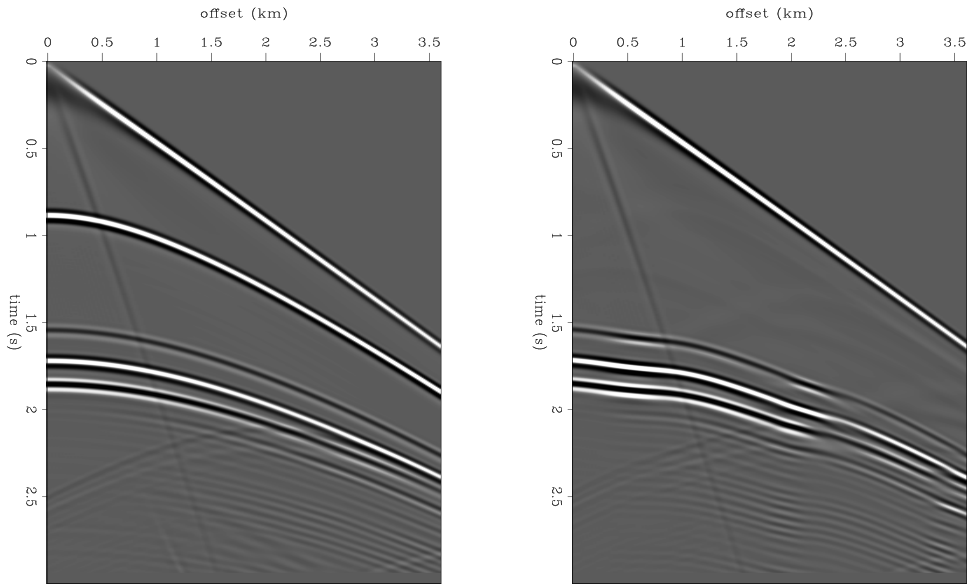

Figure 2: Shot gather at in-line location=5 km. Left: model 1, Right: model 2 cmora1-shot [CR]

Preprocessing

Divergence correction, coherent noise suppression, and CMP sorting were applied to the data before 2-D prestack depth migration. In order to compensate for spherical divergence, we scaled the data in the time axis using a function trace(t)= trace(t)*t. Coherent noise suppression was also applied to eliminate the P-wave and S-wave first arrivals. To eliminate the P-wave first arrival, we applied a linear outer mute to the data. The S-wave arrival was suppressed by applying a 2-D dip filter. Finally, the data was windowed to extract the CMPs with maximum

offset coverage and sorted by CMP location. Figure 3 shows the zero-offset section of the resulting data.

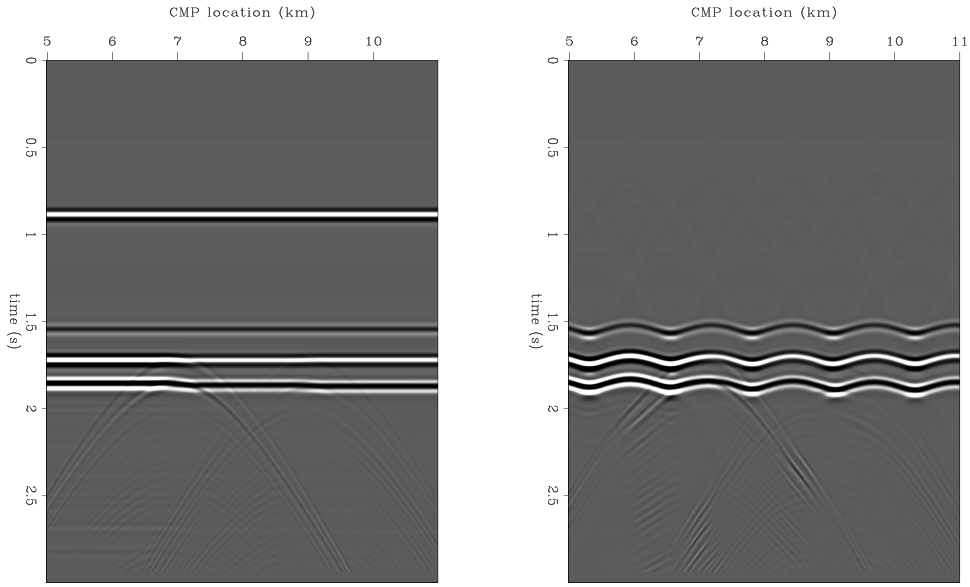

Figure 3: Zero-offset section of the resulting synthetic data. Left: model 1, Right: model 2 cmora1-zero-off [CR]

PRESTACK MIGRATION

From the original velocity model, we generated several velocity model realizations by applying a percentile perturbation at the overburden zone. Using each velocity realization, we applied a 2-D prestack wave-equation migration (Prucha et al., 1999) to the synthetic data. The resulting image is a function of the offset ray parameter p_{hx}, which is related to the aperture angle θ, the dip ϕ along the in-line direction, and the velocity function $V(z,m)$, as follows:

$$p_{hx} = \frac{2\sin\theta\cos\phi}{V(z,m)} \tag{1}$$

Figure 4 shows the result of applying prestack wave-equation migration to the synthetic data, using the original velocity models (0% perturbation) .

AVO INVERSION

The physical relation between the variation of reflection/transmission coefficients with incident angle (and offset) and rock parameters has been widely investigated. This relation is established in the Zoeppritz equations, which relate reflection and transmission coefficients for plane waves and elastic properties of the medium. Because of the nonlinearity of the Zoeppritz equations, several approximations have been generated, such as those presented by

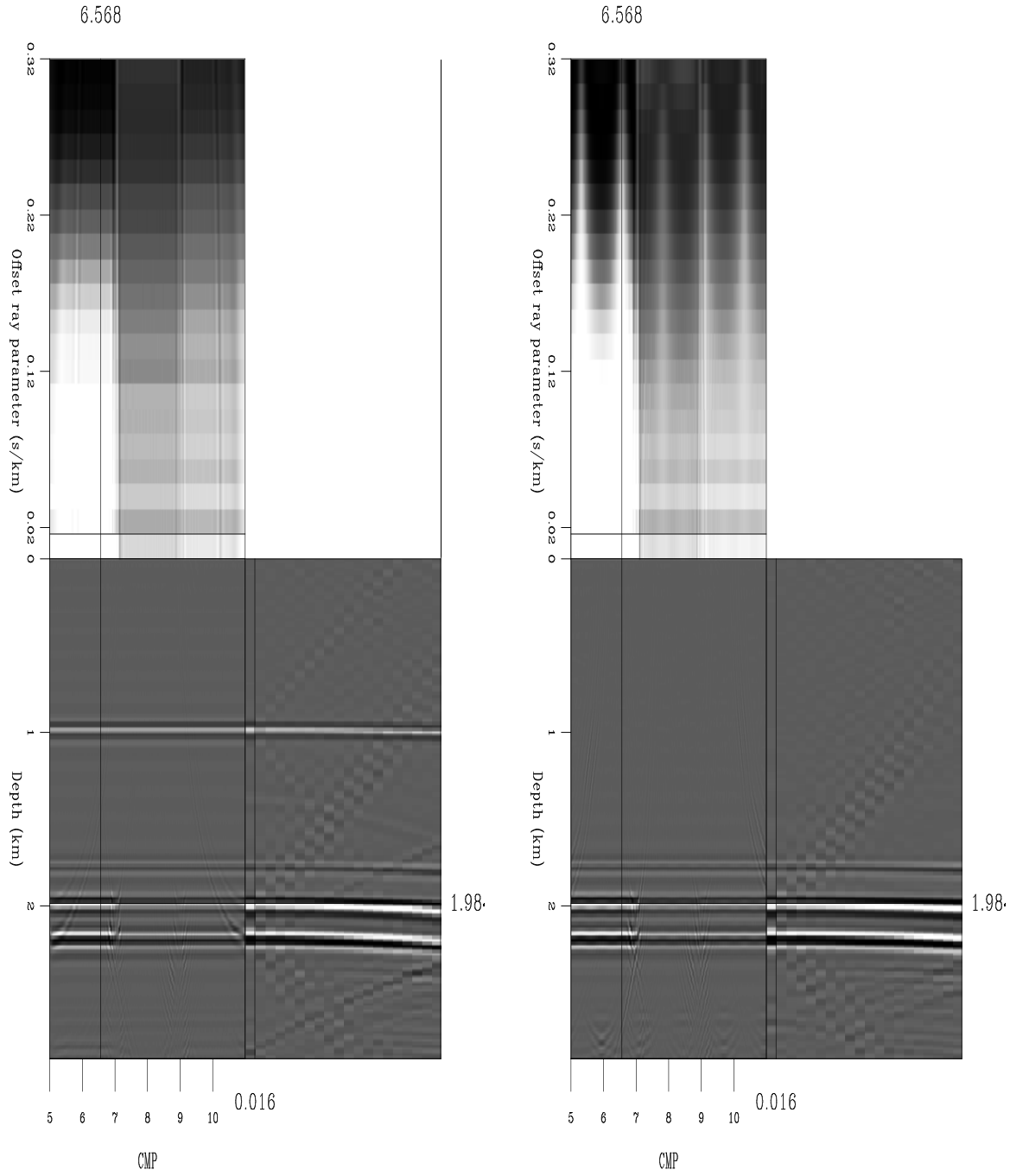

Figure 4: Result of applying prestack wave-equation migration to the synthetic data using the original velocity model. Left: model 1, right: model 2. cmora1-mig [CR]

Aki and Richards (1997) and Shuey (1985). The simplified versions of Zoeppritz equations allow the computation of AVO inversion to estimate elastic parameters from the observed reflection amplitude variation with angle. Equation (2) from Castagna and Smith (1994) is a version of Shuey's approximation for the P-wave reflection coefficient as a function of angle of incidence, which is linear in $\sin^2\theta$. This equation characterizes the reflection coefficient, at normal incidence, and at intermediate angles ($0 < \theta < 30$ degrees),

$$R(\theta) \approx A + B\sin^2\theta \tag{2}$$

$$A = \left(\frac{\Delta V_p}{V_p} + \frac{\Delta\rho}{\rho}\right)/2 \tag{3}$$

$$B = \left(-2\frac{V_s^2}{V_p^2}\frac{\Delta\rho}{\rho} + \frac{\Delta V_p}{2V_p} - 4\frac{V_s^2}{V_p^2}\frac{\Delta V_s}{V_s}\right) \tag{4}$$

where

$V_p = (V_{p2} + V_{p1})/2,$

$V_s = (V_{s2} + V_{s1})/2,$

$\rho = (\rho_2 + \rho_1)/2,$

$\Delta V_p = V_{p2} - V_{p1},$

$\Delta V_s = V_{s2} - V_{s1},$

$\Delta\rho = \rho_2 - \rho_1.$

The normal incident term, A, is commonly referred to as the AVO intercept attribute, the intermediate angles term, B, is referred to as the AVO gradient attribute. We use this approximation to invert for the intercept and gradient AVO attributes from the observed reflection amplitude variation with angle in the angle-domain common image gathers (CIG). In this domain, we pick the amplitude values at the reflector of interest and fit the amplitude versus $\sin^2\theta$ to a best straight-line approximation using a least-squares curve fitting method.

Providing a reference for the expected AVO response for the shale/brine, shale/oil, and shale/tuff interface, Figure 5 shows the P-wave reflection coefficient from the exact Zoeppritz equations. At the near offset we expect a similar reflection coefficient (similar intercept attribute) for the shale/oil and the shale/tuff interfaces because of similar acoustic impedance; however this ambiguity can be resolved by the different radio between V_s and V_p (different gradient attribute). Although this calculation is valid only for a 2-layer model, it will be a reference for the expected tendency in the modeled data. Deviation from this tendency should be due to modeling effect, overburden effect, migration operator effect, velocity anomalies effect, and migration-velocity errors. We examined the modeling effect using a 1-D, 2-layer synthetic model, the overburden and migration operator effects using model 1 (overburden with flat interface), and then we use model 2 (overburden with sinusoidal interface) to understand the effect of velocity anomalies and migration-velocity errors.

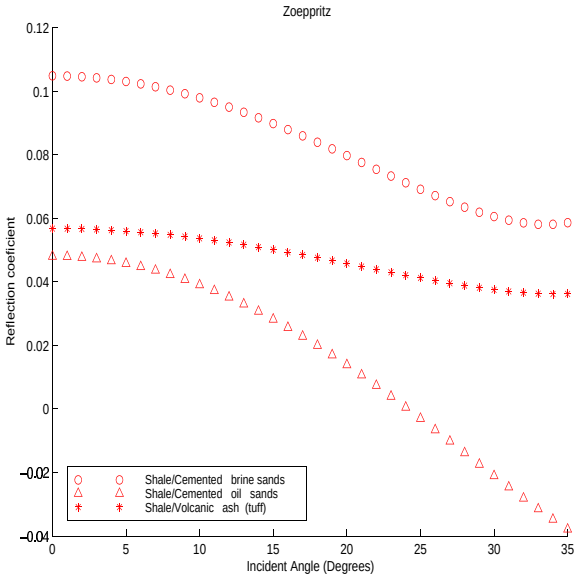

Figure 5: P-wave reflection coefficient from Zoeppritz equations cmora1-zoeppritz [CR]

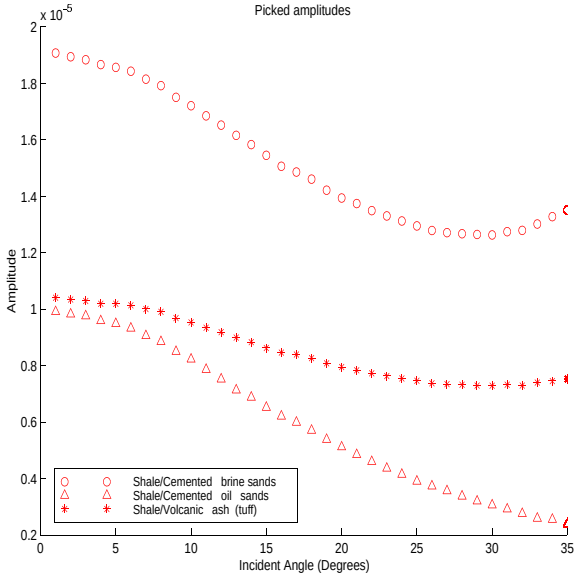

Figure 6: Picked amplitudes for a 2-layer modeling case cmora1-2laypick [CR]

Modeling effect

Illustrating the effect of the modeling in the amplitudes, Figure 6 shows the picked amplitudes (without any calibration) corresponding to a 2-layer modeling case (no overburden). Comparing this figure with Figure 5, we can see a very good qualitative agreement between the relative amplitudes of the different interfaces (shale/brine, shale/oil, and shale/tuff) and the corresponding reflection coefficients. We can see some difference for incident angles > 25 degrees; for this reason, and because Shuey's approximation is valid for incident angles < 30 degrees (see Figure 7), we will restrict the data to be used for the AVO inversion up to 25 degrees of incident angle.

We can also notice that Zoeppritz equation predicts a polarity change for the shale/oil case. We observed the same polarity change in the data (see Figure 8); however, this is not present in the picked amplitudes because we are using an automated picking program that picks the maximum absolute value in a moving window in time. We consider the automatic picking still valid in this modeling case because the polarity change is evident in the data after offset > 2 km, which corresponds to angles > 27 degrees, and we used angles up to 25 degrees for the AVO inversion. We did not use the automatic picking on migrated data, where the events are supposed to be flattened by the migration; rather, in this case, we followed the constant time corresponding to the event.

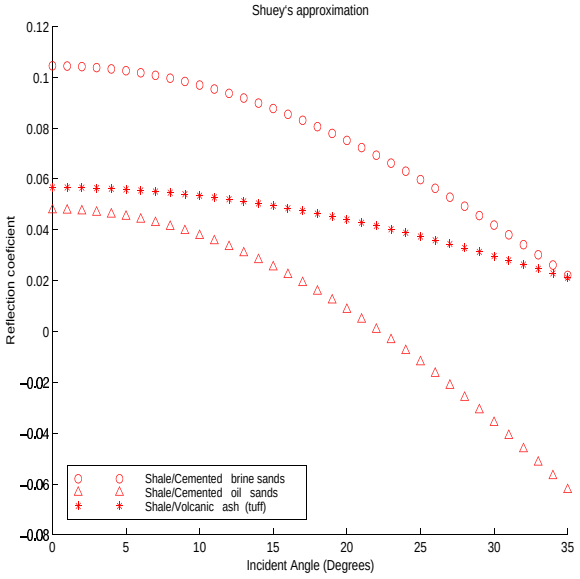

Figure 7: Shuey's approximation of P-wave reflection coefficient cmora1-shuey [CR]

Overburden effect

We used model 1 to understand the effect of the overburden in the resulting amplitudes. We compared the amplitudes of the 2-layer case to the amplitudes in model 1, which includes an overburden zone with 2 flat layers and a target zone encased in shale (see top of Figure 1). The picked amplitudes at the top of the target zone (2 km depth) are plotted in Figure 9; note the good agreement with the results illustrated in Figure 6 corresponding to the 2-layer case.

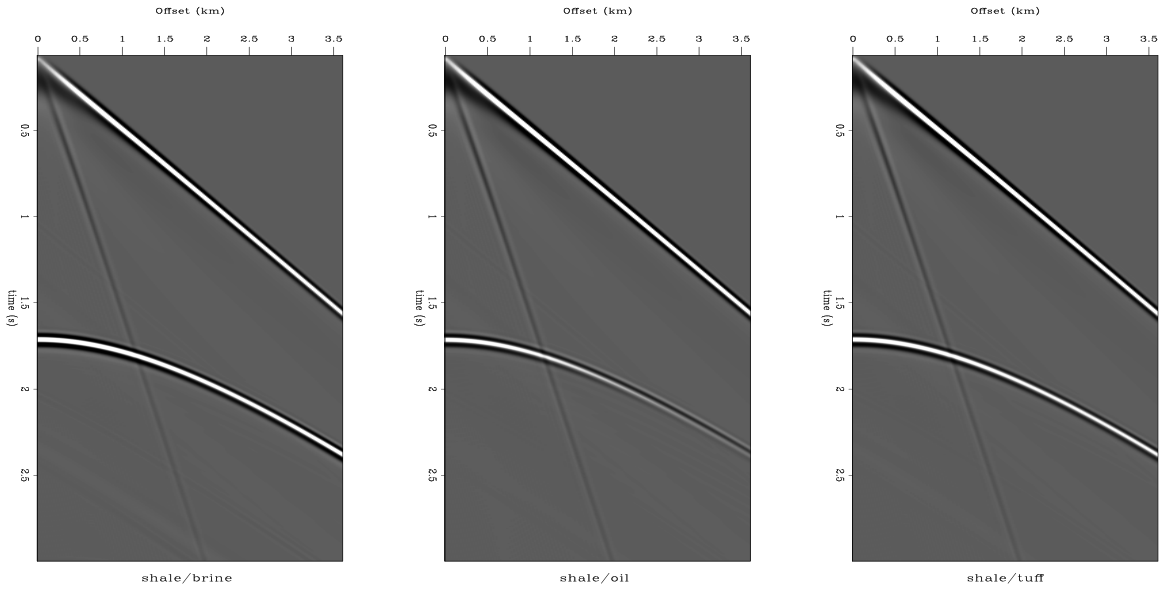

Figure 8: Modeling of shot gather for a shale/brine, shale/oil, and shale/tuff interfaces (1-D, 2-layer model). Notice the change in polarity for offset > 2 km in the shale/oil case cmora1-2lay_all [CR]

The amplitudes in model 1 are slightly higher, which can be expected because in this case the reflector appears at a higher time and the spherical divergence correction that we are applied increases the amplitudes more at a higher time (without the velocity taken into account). To confirm this, we picked the amplitudes before any preprocessing and they are identical at the near offset. We also expected some differences at the far offsets due to the AVO effect of the additional layers in model 1 (overburden effect).

Using Equation (2), we calculated the intercept (A) and gradient (B) attributes from the picked amplitudes in model 1 by fitting the amplitude versus $\sin^2\theta$ values to a straight-line approximation using a least-squares curve fitting method. Figure 11 shows the crossplot of the resulting intercept and gradient attributes; note the good quantitative agreement with Figure 10, which illustrates the theoretical values from Shuey's approximation.

Migration effect

We applied the 2-D prestack wave-equation to the synthetic data corresponding to model 1 (overburden with flat interface) using the original velocity model and picked the amplitudes at the top of the target zone in the resulting angle domain CIG. Figure 13 shows the resulting amplitudes as a function of the aperture angle at CIG locations corresponding to each lithology. The aperture angle was calculated from the offset ray parameter p_{hx} using Equation (1), with $\phi = 0$ and $V(z,m) =$ the interval velocity at the interface. We can observe some irregularities in the amplitudes values after migration. Figure 12 shows the intercept and gradient attribute calculated for each CIG. We can notice some artifacts in the data related with boundary effects;

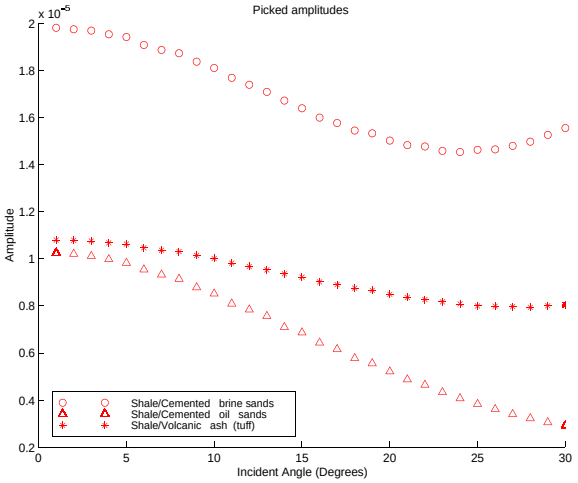

Figure 9: Picked amplitudes from model 1 cmora1-model1pick [CR]

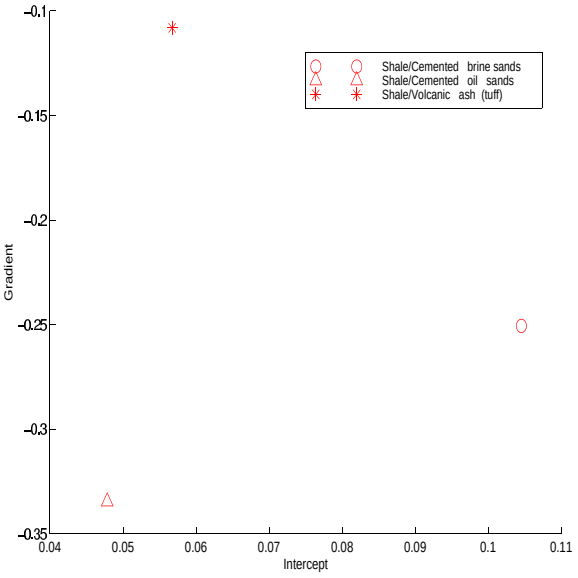

Figure 10: Intercept versus Gradient crossplot from Shuey's approximation of P-wave reflection coefficient cmora1-ABshuey [CR]

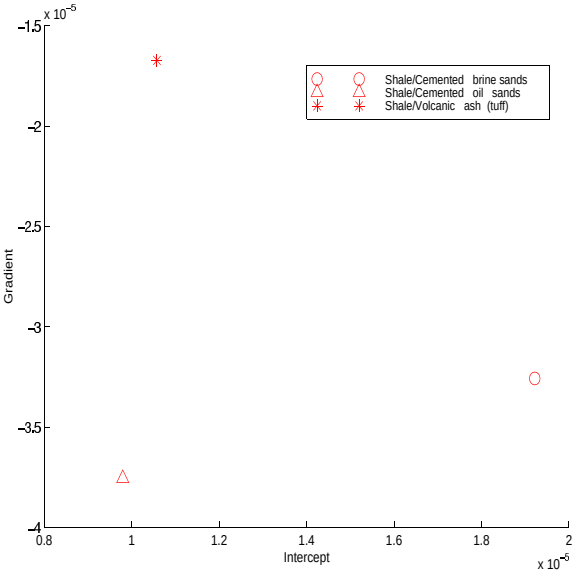

Figure 11: Intercept versus Gradient crossplot from picked amplitudes in data model 1 before migration cmora1-ABmodel1 [CR]

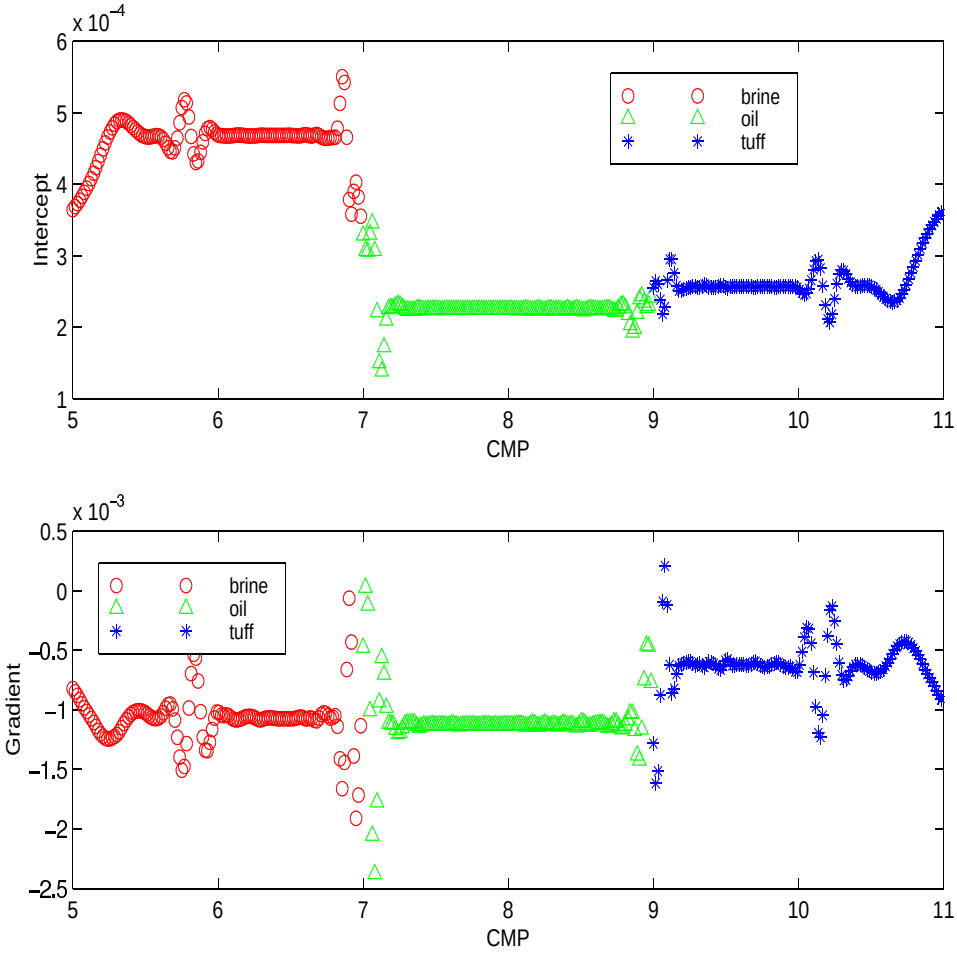

Figure 12: Variability of intercept and gradient attribute along the different CIGs of model 1 cmora1-ABmodel1_var [CR]

these artifacts are very strong at the edges of the model and at the lateral interfaces between the different lithologies at the target zone. Even though the CIGs used for Figure 13 were taken from locations where we noted less variability, these artifacts could be affecting the amplitudes.

Figure 14 shows the crossplot of the inverted intercept and gradient attributes for the same CIG locations used for Figure 13. The relative intercept and attribute values for the different lithologies are in good agreement with the expected tendency, however, we can note from Figure 12 that this will not be the case if the CIG's are chosen close to the boundary artifacts.

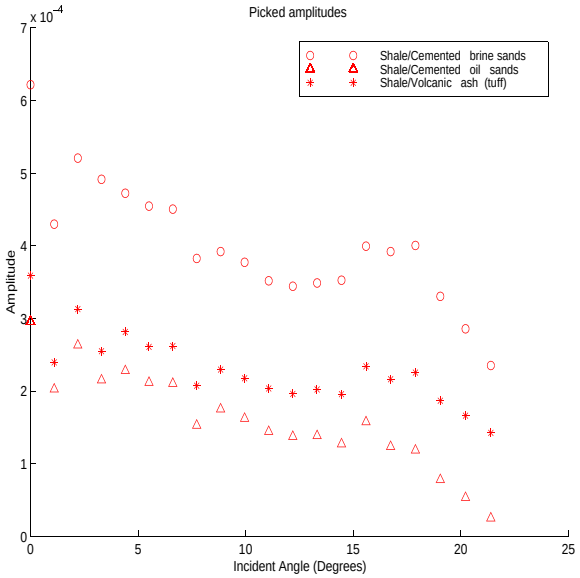

Figure 13: Picked amplitudes from CIG of model 1 cmora1-model1migpick [CR]

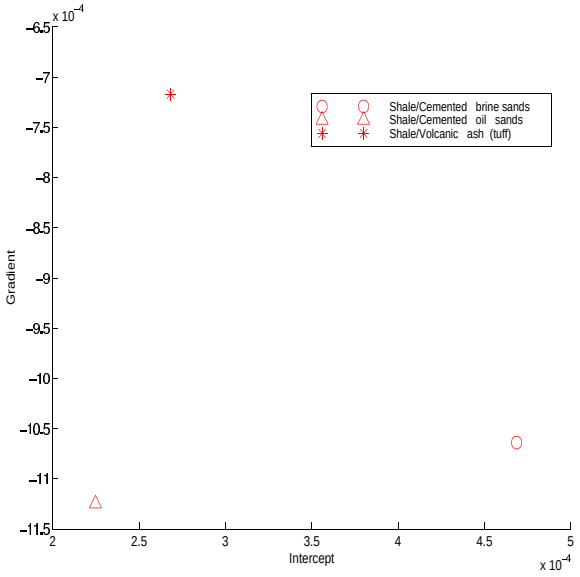

Figure 14: Intercept versus Gradient crossplot from picked amplitudes of model 1 after migration cmora1-ABmodel1mig [CR]

Velocity anomalies effect

In this case, we applied the 2-D prestack wave-equation to the synthetic data corresponding to model 2 (overburden with sinusoidal interface) using the original velocity model. We modeled and migrated the data using 1 more km on each side of the inline axis to avoid the edge artifacts at the boundary of the model, but the edge artifacts corresponding to the lateral boundaries between brine-oil and oil-tuff lithologies are still present. Figure 15 shows the picked the amplitudes at the top of the target zone in the migrated CIG. Note how the intercept and gradient change follow the sinusoidal velocity anomalies. Figure 16 shows the picked amplitudes

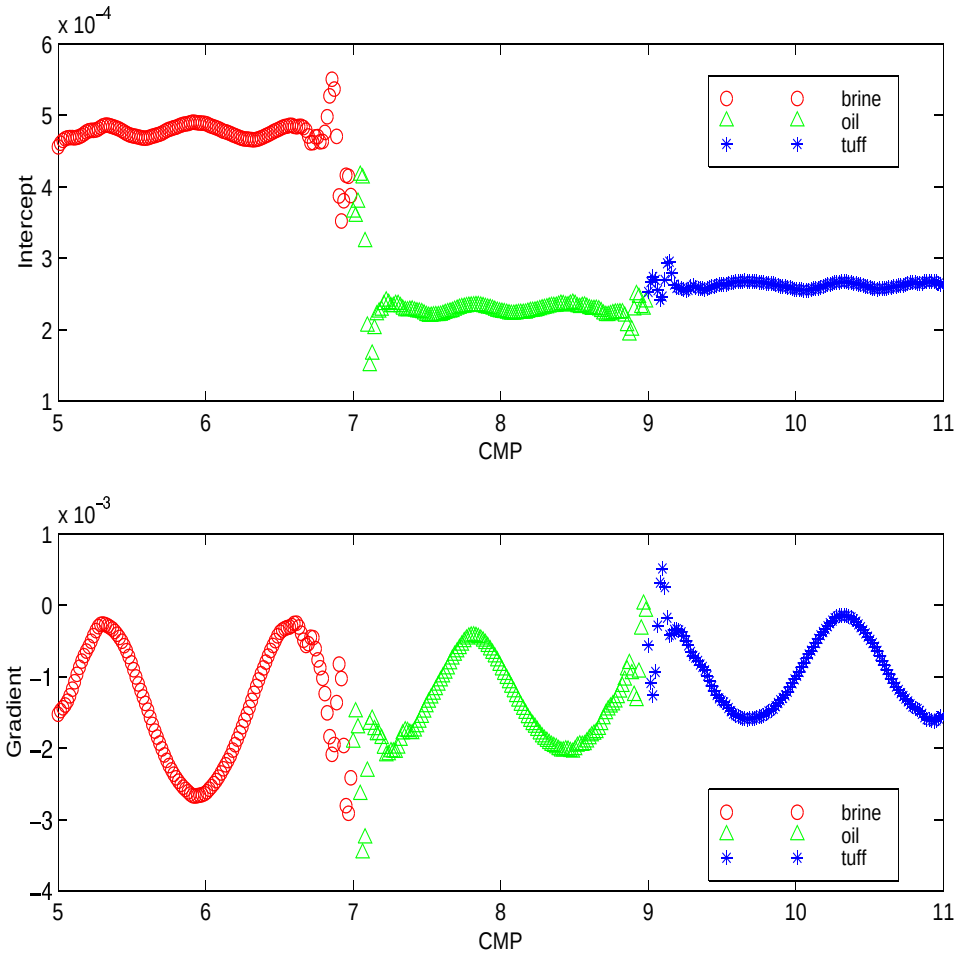

Figure 15: Impact of velocity anomalies in intercept and gradient attribute cmora1-AB_var [CR]

at the CIG locations, which correspond to a valley of the sinusoidal irregularities (where the event was observed to be flatter) for each lithology (positions 6.576, 7.824, and 10.304), and Figure 17 shows the crossplot of the corresponding intercept and gradient attributes. In both cases, we can observe a good agreement with the expected tendencies. We also calculated the intercept and gradient attributes at CIGs locations which correspond to a peak of the sinusoidal irregularities; in this case, the relative gradient value for the shale/brine interface is higher than

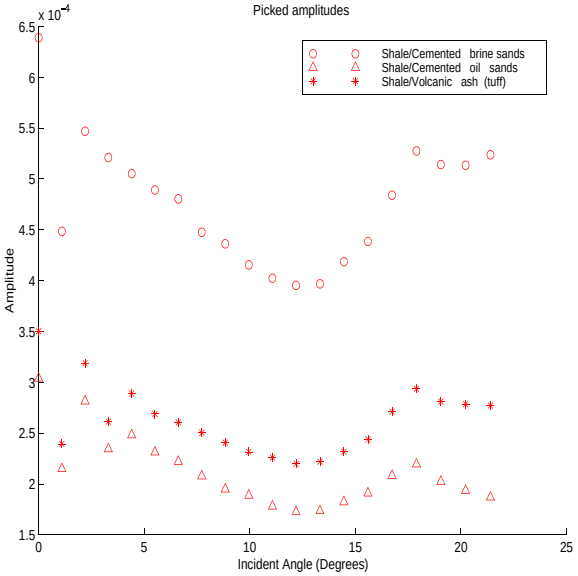

Figure 16: Picked amplitudes from CIG of model 2 cmora1-model2migpick [CR]

expected.

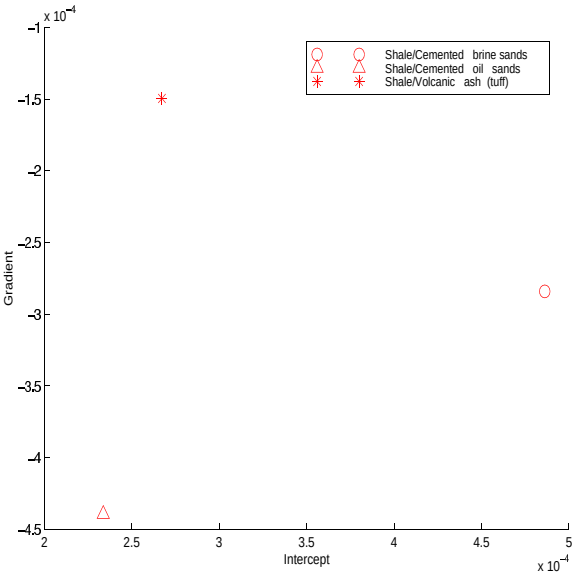

Figure 17: Intercept versus Gradient crossplot from picked amplitudes of model 2 after migration cmora1-ABmodel2mig [CR]

Velocity errors effect

Using the synthetic data corresponding to model 2, we generated several migration-velocity realizations by introducing coherent percentage velocity errors at the overburden zone of the original velocity model. Using each velocity realization, we applied 2-D prestack wave-equation migration to the synthetic data; we applied an additional residual moveout correction and picked the resulting amplitudes. Figure 18 shows the crossplot of the intercept and gradient attributes at CIGs location which correspond to a valley of the sinusoidal irregularities; the

size in the plot symbol increases as the velocity error increases. We can note that the intercept attribute is much less sensitive to velocity errors than the gradient attribute. Figure 19 shows the errors in the inverted attributes as a function of the velocity errors used in the migration. We can see that the maximum AVO intercept error is 34% for velocity errors up to 5% (tuff case), whereas for velocity errors of only 1%, the inversion of AVO gradient attribute (brine case) has an error of 185%.

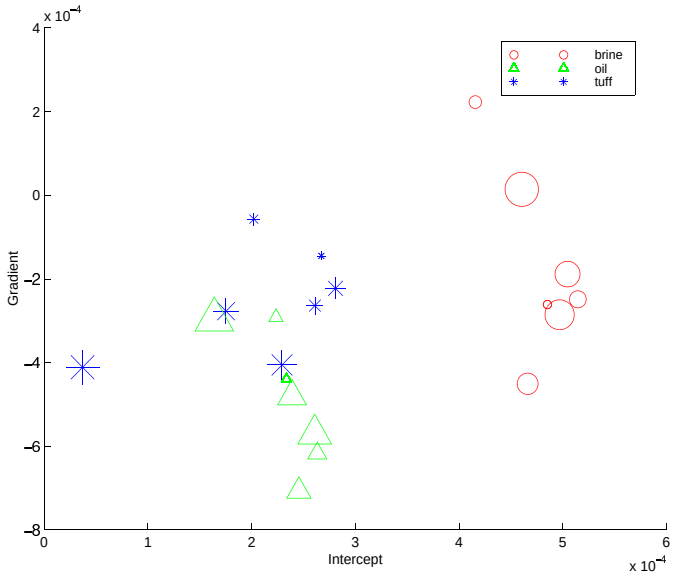

Figure 18: Impact of velocity errors in Intercept versus Gradient crossplot cmora1-mig_vel [CR]

CONCLUSION

We examined the sensitivity of the AVO response due to the presence of a overburden with complex velocity anomalies using a synthetic data set. We observed that AVO attributes calculated after prestack depth migration using the true velocity model are sensitive to the velocity anomalies. Introducing errors in the migration-velocity, we found that the AVO gradient attribute is much more sensitive to velocity errors than AVO intercept attribute. For velocity errors up to 5%, we can see a maximum of AVO intercept errors of 34%, whereas for velocity errors of only 1%, the inversion of AVO gradient attribute has an error of 185%. These results are specific for the synthetic data used; different results could be obtained by modeling different velocity anomalies.

We observed some boundary artifacts in the modeled data and we noted that amplitude values after migration are more sensitive to these boundary artifacts than amplitude values before migration. These boundary artifacts become worse when we introduce velocity errors in the migration-velocity. We need to do further work to evaluate the influence of boundary artifacts on the amplitudes; we also would like to compare the results using other migration methods, such as Kirchhoff prestack migration.

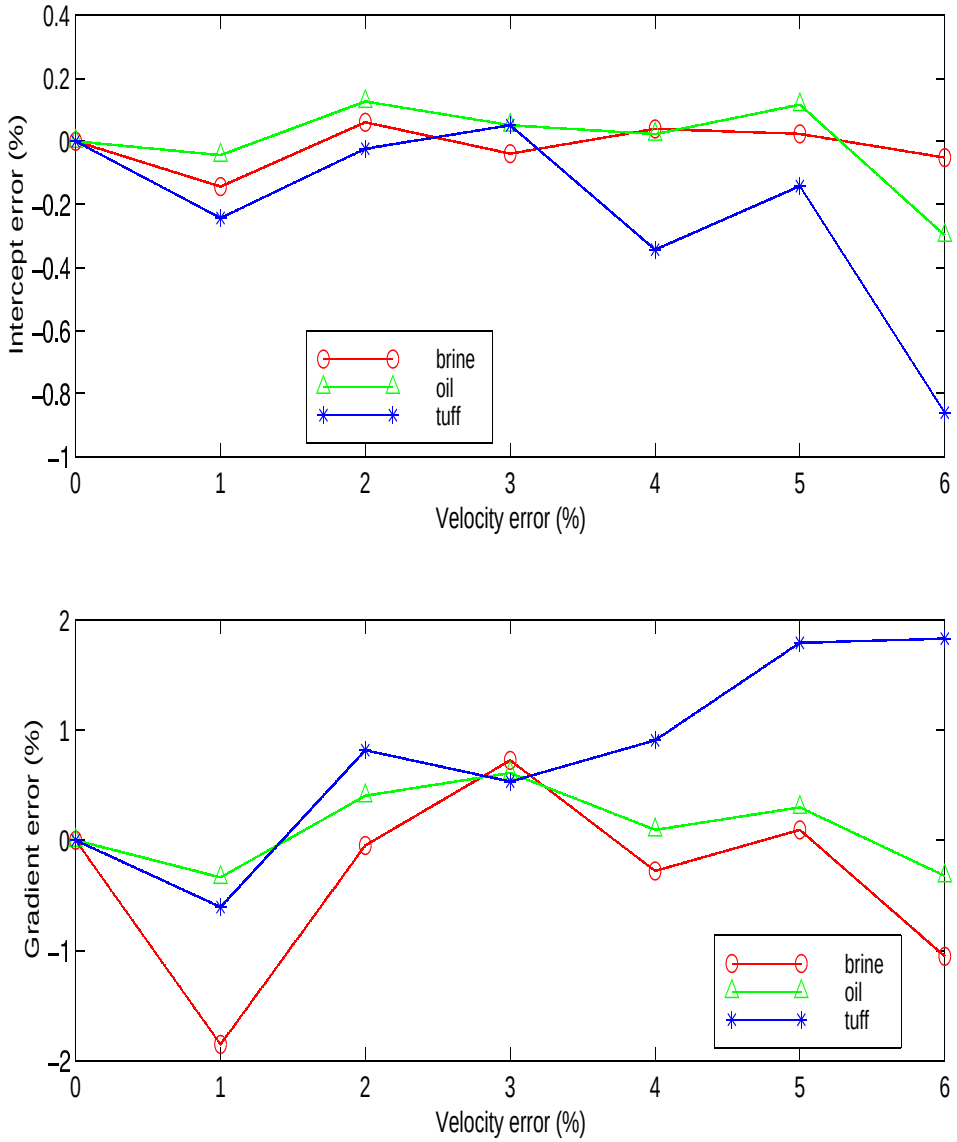

Figure 19: Impact of velocity errors in Intercept and gradient attributes cmora1-AB_error [CR]

ACKNOWLEDGMENTS

We gratefully acknowledge James Rickett and Antoine Guitton for their many helpful suggestions and discussions. We also would like to thank Per Avseth for providing the earth model properties used for the modeling and Robert Clapp for his support during the development of this work.

REFERENCES

Aki, K. I., and Richards, P. G., 1997, Quantitative seismology: Theory and methods: W. H. Freeman and Company, New York.

Avseth, P., Mavko, G., Mukerji, T., and Tyssekvam, J., 1999, Integrating seismic lithofacies prediction and depositional geometry analysis for reservoir delineation in a north sea turbidite field: 69th Annual Internat. Mtg., Soc. Expl. Geophys., Expanded Abstracts, 752–755.

Castagna, J. P., and Smith, S. W., 1994, Comparison of avo indicators: A modeling study: Geophysics, **59**, no. 12, 1849–1855.

Grubb, H., and Tura, A., 1997, Interpreting uncertainty measures for AVO migration/inversion: 67th Annual Internat. Mtg., Soc. Expl. Geophys., Expanded Abstracts, 210–213.

Mora, C., and Biondi, B., 1999, Seismic attribute sensitivity to velocity uncertainty: SEP–**102**, 157–176.

Ostrander, W. J., 1984, Plane-wave reflection coefficients for gas sands at nonnormal angles of incidence: Geophysics, **49**, no. 10, 1637–1648.

Prucha, M. L., Biondi, B. L., and Symes, W. W., 1999, Angle-domain common image gathers by wave-equation migration: SEP–**100**, 101–112.

Shuey, R. T., 1985, A simplification of the Zoeppritz equations: Geophysics, **50**, no. 4, 607–614.

Swan, H. W., 1993, Properties of direct AVO hydrocarbon indicators *in* Castagna, J. P., and Backus, M. M., Eds., Offset dependent reflectivity — Theory and practice of AVO analysis:: Society of Exploration Geophysics, 78–92.